Hydrogen-Bond-Assisted Solution Discharge in Aprotic Li–O₂ Batteries

Qi Xiong, Chaole Li, Ziwei Li, Yulong Liang, Jianchen Li, Junmin Yan, Gang Huang,* and Xinbo Zhang*

Surface discharge mechanism induced cathode passivation is a critical challenge that blocks the full liberation of the ultrahigh theoretical energy density in aprotic Li–O₂ batteries. Herein, a facile and universal concept of hydrogen-bond-assisted solvation is proposed to trigger the solution discharge process for averting the shortcomings associated with surface discharge. 2,5-Di-tert-butylhydroquinone (DBHQ), an antioxidant with hydroxyl groups, is introduced as an exemplary soluble catalyst to promote solution discharge by hydrogen-bond-assisted solvation of O_2^- and Li_2O_2 (O—H···O). Thus, a Li–O₂ battery with 50×10^{-3} M DBHQ delivers an extraordinary discharge capacity of 18 945 mAh g^{-1} (i.e., 9.47 mAh cm^{-2}), even surpassing the capacity endowed by the state-of-the-art reduction mediator of 2,5-di-tert-butyl-1,4-benzoquinone. Besides, an ultrahigh Li_2O_2 yield of 97.1% is also achieved due to the depressed reactivity of the reduced oxygen-containing species (O_2^-, LiO_2, and Li_2O_2) by the solvating and antioxidative abilities of DBHQ. Consequently, the Li–O₂ battery with DBHQ exhibits excellent cycling lifetime and rate capability. Furthermore, the generalizability of this approach of hydrogen-bond-assisted solution discharge is verified by other soluble catalysts that contain —OH or —NH groups, with implications that could bring Li–O₂ batteries one step closer to being a viable technology.

1. Introduction

Since the rechargeable Li–O₂ battery was proposed by Abraham in 1996,[1] it has aroused the interest of lots of scientists for its extremely high theoretical gravimetric energy density (3460 Wh kg^{-1}).[2] The typical reaction equation of the aprotic

Q. Xiong, C. Li, Z. Li, Y. Liang, J. Li, J. Yan
Key Laboratory of Automobile Materials
Ministry of Education
Department of Materials Science and Engineering
Jilin University
Changchun 130022, China
Q. Xiong, C. Li, Z. Li, Y. Liang, G. Huang, X. Zhang
State Key Laboratory of Rare Earth Resource Utilization
Changchun Institute of Applied Chemistry
Chinese Academy of Sciences
Changchun 130022, China
E-mail: ghuang@ciac.ac.cn; xbzhang@ciac.ac.cn
X. Zhang
University of Science and Technology of China
Hefei 230026, China

Li–O₂ battery is $2Li + O_2 \rightleftharpoons Li_2O_2$, in which O_2 is reduced on the cathode with the formation of Li_2O_2 during discharge, and the discharge capacity can be easily influenced by the discharge mechanisms. Generally, there are two discharge routes for the growth of Li_2O_2, surface electrochemical pathway and solution-mediated electrochemical pathway, which are governed by the solubility of LiO_2 in the electrolyte.[3] During the discharge by surface pathway, O_2 is first reduced to O_2^- through one-electron reduction (Equation (1)), then the O_2^- adsorbed on the cathode will combine with Li^+ to produce LiO_2 (Equation (2)). Finally, the adsorbed LiO_2 will continually undergo a second electron reduction (Equation (3)),[3,4] forming thin-film Li_2O_2 with rapid passivation of the cathode, and eventually making the Li–O₂ battery deliver a low discharge capacity and poor rate capability.

$$O_2 + e^- \rightarrow O_2^-* \tag{1}$$

$$O_2^-* + Li^+ \rightarrow LiO_2 * \tag{2}$$

$$LiO_2 * + e^- + Li^+ \rightarrow Li_2O_2 \tag{3}$$

For the solution-mediated pathway on discharge, the reduced O_2^- from one-electron reduction will dissolve in the electrolyte (Equation (4)), then the solvated O_2^- combines with Li^+ (Equation (5)) and subsequently undergoes a disproportionation reaction (Equation (6)),[3–5] precipitating Li_2O_2 as large toroidals with high discharge capacity and excellent rate capability.

$$O_2 + e^- \rightarrow O_{2(sol)}^- \tag{4}$$

$$O_{2(sol)}^- + Li^+ \rightarrow LiO_{2(sol)} \tag{5}$$

$$2LiO_{2(sol)} \rightarrow Li_2O_2 + O_2 \tag{6}$$

In order to unlock the ultrahigh specific energy density of Li–O₂ battery, the solution-mediated pathway on discharge is preferred and accordingly many efforts have been made to accelerate this pathway in Li–O₂ batteries. For example, reduction mediators, like 2,5-di-tert-butyl-1,4-benzoquinone (DBBQ)[6] and coenzyme Q_{10},[7] have been proposed as the electron shuttle to transfer electrons from the electrode to O_2,[6–8] shifting the

**ADVANCED
SCIENCE NEWS**

www.advancedsciencenews.com

**ADVANCED
MATERIALS**

www.advmat.de

oxygen reduction reaction (ORR) sites from the cathode surface to electrolyte solution to facilitate the solution discharge process. High-donor-number (DN) or high-acceptor-number (AN) electrolytes/additives which can respectively increase the solubility of Li^+ or O_2^-,[3,9] and additives that can capture O_2^- or LiO_2,[10] will also result in a dominance of the solution discharge pathway. Moreover, protic additives, such as H_2O and phenol,[11] can likewise induce the solution discharge by forming the protonated intermediate (lithium hydroperoxide, LiOOH).[2e,11b,c] Though the above studies have achieved some success, it is still difficult to quickly screen a new solvent or additive that could promote the solution discharge of $Li–O_2$ battery, given that the data of physical and chemical parameters or redox properties of the solvent or additive cannot be easily accessed. Therefore, developing a facile unified method will pave the way to rapidly screen a class of functional additives for triggering the solution discharge pathway in $Li–O_2$ battery.

Hydrogen bonds (X—H$\cdots$Y, X and Y represent highly electronegative atoms, such as N, O, and F),[12] widely exist in the natural world, could increase the attractive interaction between two molecules. Coincidentally, both the discharge intermediates and product (O_2^-, LiO_2, and Li_2O_2) of the $Li–O_2$ battery possess highly electronegative O atoms, so we could venture a guess that the hydrogen bonding interaction could increase the solubility of these reduced oxygen-containing species (O_2^-, LiO_2, and Li_2O_2) in the electrolytes with molecules containing X—H group, and thus resulting in a solution discharge pathway. To realize this, the molecules should be stable against the nucleophilic attacks from the reduced species. Antioxidants, widely used in the food industry, that can inhibit the oxidation of organics by stabilizing the free radicals, would be good choices.[13] Therefore, an excellent antioxidant with hydroxyl group (—OH) could not only withstand the harsh operating environment in the $Li–O_2$ battery by stabilizing the reactive free radicals (O_2^- and LiO_2), but also increase the solubility of the reduced oxygen-containing species (O_2^-, LiO_2, and Li_2O_2) via hydrogen-bond-assisted solvation to promote the solution discharge. However, the potential functions of the hydrogen bonds and antioxidants in $Li–O_2$ batteries have rarely been investigated, so exploration works are required to unearth their mysterious efficacy.

In this work, 2,5-di-tert-butylhydroquinone (DBHQ), a superb antioxidant and inhibitor with hydroxyl groups,[13] is introduced as a soluble catalyst to reinforce the solution discharge process and alleviate the decomposition of the electrolytes by the strongly oxidative and aggressive reduced oxygen-containing species (O_2^-, LiO_2, and Li_2O_2) in $Li–O_2$ batteries. The high solvating ability of the hydroxyl groups in DBHQ is able to well solvate O_2^- and Li_2O_2 by hydrogen bonding interaction (O—H$\cdots$O), and bind with Li^+ and LiO_2 through electrostatic attraction. Therefore, in the presence of 50×10^{-3} M DBHQ, the $Li–O_2$ battery can promote the solution discharge with a prominent rate capability and an ultrahigh discharge capacity of 18 945 mAh g^{-1} (i.e., 9.47 mAh cm^{-2}) at a current density of 200 mA g^{-1}, comprehensively outperforming the performance of the state-of-the-art reduction mediator of 2,5-di-tert-butyl-1,4-benzoquinone (DBBQ). Moreover, the uniquely solvating and antioxidative efficacies of the DBHQ empower it to stabilize the reactive reduced oxygen-containing species (O_2^-, LiO_2,

and Li_2O_2), thus alleviating the parasitic reactions in the $Li–O_2$ battery and yielding an ultrahigh Li_2O_2 generation efficiency of 97.1%. As a result, the $Li–O_2$ battery with DBHQ achieves a long operation lifetime of 161 cycles. This hydrogen-bond-assisted solution discharge approach can be applied to other additives with —OH or —NH groups, endowing the $Li–O_2$ batteries with large discharge capacities.
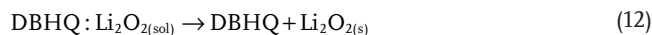
2. Results
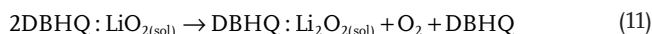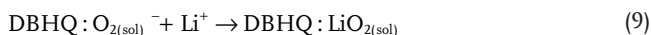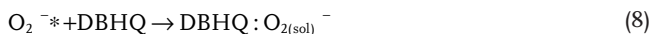
Like the hydrogen bonding interaction in the natural world, the electron-deficient H atom of the hydroxyl groups (—OH) in DBHQ is hypothesized to form hydrogen bonds (O—H$\cdots$O) with the strongly electronegative O atoms of the reduced oxygen-containing species (O_2^-, LiO_2, and Li_2O_2) in $Li–O_2$ battery. To determine whether DBHQ can promote the solution discharge in $Li–O_2$ battery, density functional theory (DFT) calculations were first conducted by Gaussian 16A[14] and Multiwfn[15] softwares to demonstrate the potential solvating ability of DBHQ toward the reduced oxygen-containing species (O_2^-, LiO_2, and Li_2O_2) and Li^+. The molecular electrostatic potential (MESP) maps are shown in **Figure 1**a–c. It is clear that the surface minima and maxima of the MESP for DBHQ appear on the O and H atoms of the hydroxyl groups (Figure 1a; Figure S1, Supporting Information), and the negative and positive MESP values of the Li_2O_2 and LiO_2 mainly locate around the O and Li atoms (Figure 1b,c), respectively. Hence, we can reasonably assume that the electron-rich O atoms of the O_2^-, LiO_2, and Li_2O_2 are prone to bind with the electron-deficient H atom of the hydroxyl groups in DBHQ through hydrogen bonding interaction, or the electron-deficient Li atoms of the LiO_2, Li_2O_2, and Li^+ are apt to bind with the electron-rich O atom of the hydroxyl groups in DBHQ through electrostatic interaction. Following this, the structures of the complexes and their monomers were optimized and listed in the Supporting Information (Figures S2, S3 and Tables S1–S5, Supporting Information). According to the thermodynamic results, when DBHQ binds with O_2^-, LiO_2, Li_2O_2, and Li^+, the total Gibbs free energy changes are –0.40, –0.11, –0.68, and –0.34 eV (Figures S2d–f,S3b, Supporting Information), respectively, indicating that DBHQ can solvate these reduced oxygen-containing species and Li^+, particularly for O_2^- and Li_2O_2 through hydrogen bonding interaction (O—H$\cdots$O) in terms of the larger Gibbs free energy changes. Then electron density difference maps were employed to characterize the chemical bonds between DBHQ and reduced species/Li^+. For DBHQ:O_2^-, the electron transfers from O_2^- to the H atom of the hydroxyl groups in DBHQ due to the formation of hydrogen bond (O—H$\cdots$O) (Figure 1d), and the result well coincides with the analysis of the difference map of electron localization function (ELF), in which the electron localization near the H atom of the hydroxyl group is significantly decreased as a consequence of Pauli repulsion effect (Figure 1g). The strong hydrogen bonding interaction (O—H$\cdots$O) can be also evidenced between DBHQ and Li_2O_2 (Figure 1e,h). Besides, the difference maps of electron density and ELF also reveal that the electron-deficient Li atoms of the Li^+ and LiO_2 can interact with the electron-rich O atom of the hydroxyl groups in DBHQ through electrostatic interaction
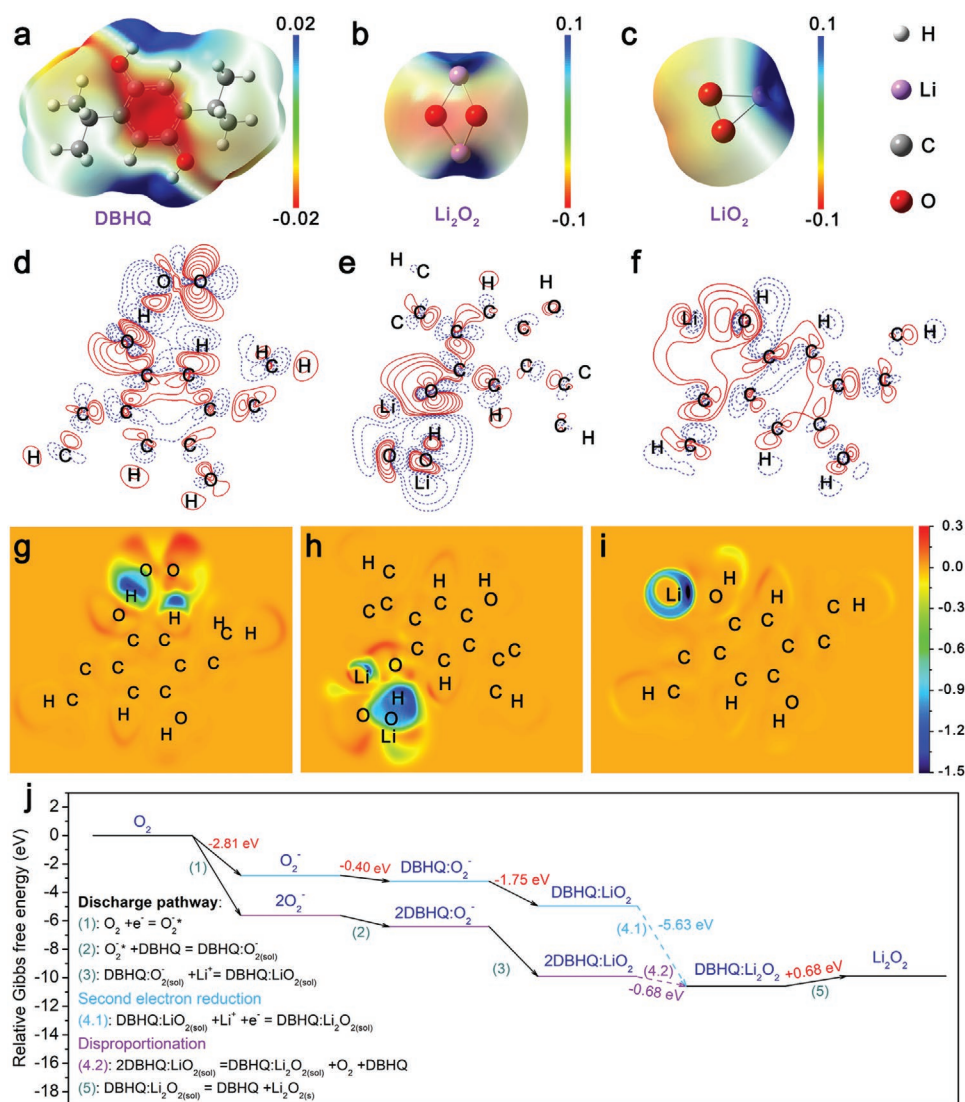
Figure 1. a–c) Isosurface maps of the MESP for DBHQ (a), Li_2O_2 (b), and LiO_2 (c). d–f) Plane maps of electron density difference and g–i) color-filled difference maps of ELF for $DBHQ:O_2^-$ (d,g), $DBHQ:Li_2O_2$ (e,h), and $DBHQ:Li^+$ (f,i) with their monomers. j) The relative Gibbs free energy changes of the DBHQ regulated discharge pathway.

(Figure 1f,i; Figure S3c,d, Supporting Information). Moreover, the changes of the Mayer bond orders and bond lengths further confirm the existence of strong interaction between DBHQ and the reduced oxygen-containing species and Li^+ (Tables S6–S9, Supporting Information).

On the basis of the thermodynamic data of the Gibbs free energy changes (Figure 1j), the DBHQ regulated discharge mechanism can be depicted as follows:

$$O_2 + e^- \rightarrow O_2^-* \tag{7}$$

$$O_2^-* + DBHQ \rightarrow DBHQ:O_{2(sol)}^- \tag{8}$$

$$DBHQ:O_{2(sol)}^- + Li^+ \rightarrow DBHQ:LiO_{2(sol)} \tag{9}$$

$$DBHQ:LiO_{2(sol)} + Li^+ + e^- \rightarrow DBHQ:Li_2O_{2(sol)} \tag{10}$$

$$2DBHQ:LiO_{2(sol)} \rightarrow DBHQ:Li_2O_{2(sol)} + O_2 + DBHQ \tag{11}$$

$$DBHQ:Li_2O_{2(sol)} \rightarrow DBHQ + Li_2O_{2(s)} \tag{12}$$

Briefly, O_2 will first undergo an one-electron reduction on the cathode with the formation of O_2^- during discharge (Equation (7)), then O_2^- will be dissolved by DBHQ (Equation (8)) and further complex with Li^+ (Equation (9)). The formed $DBHQ:LiO_2$ can either undergo a second electron reduction and subsequently combine with another Li^+ (Equation (10)) or merely experience a disproportionation reaction (Equation (11)). Eventually, the generated $DBHQ:Li_2O_2$ releases Li_2O_2 with the recovery of DBHQ (Equation (12)), and the free Li_2O_2 will tend to recrystallize into large toroidals through Ostwald ripening. In summary, the hydroxyl groups of the DBHQ induced strong interaction with the reduced oxygen-containing species and Li^+, especially for the stronger hydrogen
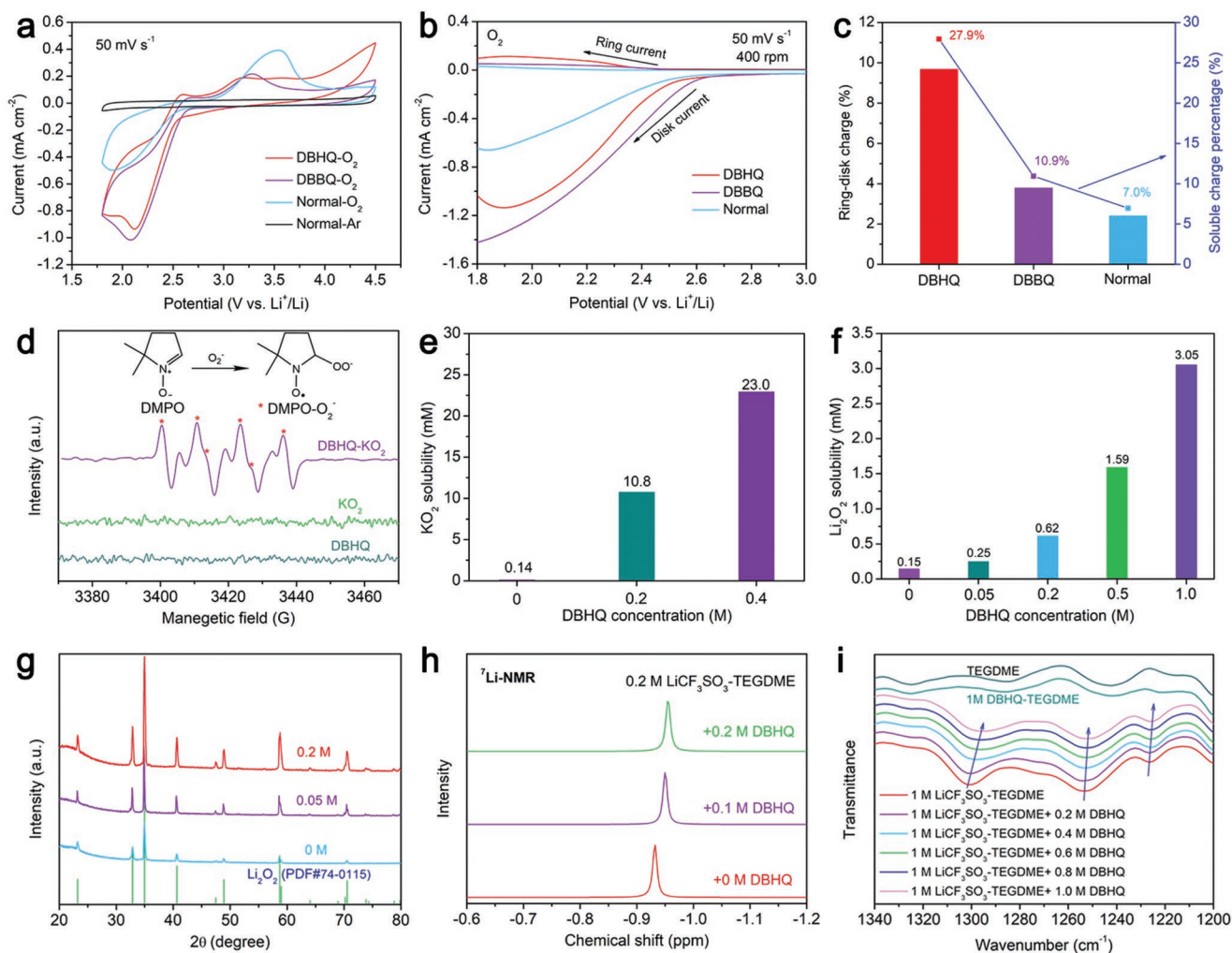
Figure 2. a) CV and b) RRDE measurements in 1 M LiCF$_3$SO$_3$-TEGDME with 5×10^{-3} M DBHQ/DBBQ and without additive under O$_2$/Ar atmosphere at a scan rate of 50 mV s^{-1}. c) The percentages of soluble ORR charge quantified by the RRDE tests. d) EPR spectra of the different electrolytes with DMPO as a radical scavenger. e,f) Quantitative analysis of the solubilities for KO$_2$ (e) and Li$_2$O$_2$ (f) in TEGDME with different concentrations of DBHQ. g) XRD patterns of the Li$_2$O$_2$ after being dissolved in TEGDME with varying DBHQ contents. h) ^{7}Li NMR and i) FT-IR spectra for the electrolytes of 0.2 M LiCF$_3$SO$_3$ in TEGDME with varying DBHQ contents.

bonding interaction (O—H···O) with O$_2^-$ and Li$_2$O$_2$, will be of vital importance to accelerate the ORR kinetics for solution-mediated discharge.

To verify the above DFT calculation results, the effects of DBHQ on the redox electrochemistry in Li–O$_2$ battery were first evaluated by cyclic voltammetry (CV) measurement in 1 M LiCF$_3$SO$_3$-tetraethylene glycol dimethyl ether (TEGDME) with and without additives (**Figure 2**a; Figures S6 and S7, Supporting Information). 2,5-Di-tert-butyl-1,4-benzoquinone (DBBQ),[6] which was once recognized as the best soluble catalyst for ORR in Li–O$_2$ battery, was also included in the scope of this study for comparison. As shown in Figure 2a, the ORR current densities are drastically enhanced in the presence of DBHQ and DBBQ, which can be ascribed to the retardance of electrode passivation by the solution-mediated discharge process. Then rotating ring-disk electrode (RRDE) tests were executed to quantify the proportion of the soluble ORR charge during discharge.[16] Since the ORR charge is composed of soluble (e.g., O$_2^-$ and LiO$_2$) and

insoluble (Li$_2$O$_2$) components, and the portion of the soluble ORR component could be oxidized on the ring electrode at 3.5 V versus Li$^+$/Li, thus the percentage of soluble ORR charge can be calculated by dividing the ring charge (Q_{ring}) into the disk charge (Q_{disk}) and the collection efficiency (η) of RRDE.[16] Though the disk current density for ORR in the electrolyte with DBHQ is slightly lower than that with DBBQ (Figure 2a,b), the ring current density in the electrolyte with DBHQ is significantly higher than that with DBBQ (Figure 2b), and the percentages of the soluble ORR charge are quantitatively estimated to be 27.9%, 10.9%, and 7.0% for the electrolytes with DBHQ, DBBQ and without additive (Figure 2c), respectively. Given that DBHQ is the hydrogenated form of DBBQ without other difference, we can presume that the greatly enhanced solution discharge pathway in the electrolyte with DBHQ can be attributed to the strong solvating ability of the hydroxyl groups (—OH).

Next, the intensified solvating ability of DBHQ toward the reduced oxygen-containing species and Li$^+$ was proved. In

order to demonstrate the existence of O_2^- in the centrifugated supernatant fluid of DBHQ and KO_2 in TEGDME, electron paramagnetic resonance (EPR) measurement was carried out to detect the unpaired electron of O_2^- and 5,5-dimethyl-1-pyrroline-*N*-oxide (DMPO) was employed as a radical scavenger. With the addition of DMPO, the EPR signals of DMPO-O_2^- adduct appear (Figure 2d),[10c-e] which strongly suggests the high solvating ability of DBHQ toward O_2^-. Then, the solubilities of the commercial KO_2 and Li_2O_2 in TEGDME with varying DBHQ contents were analyzed by the inductively coupled plasma atomic emission spectrometer (ICP-AES). It shows that the solubilities of KO_2 and Li_2O_2 increase with the concentration of DBHQ (Figure 2e,f). Besides, when centrifuging and drying the mixture of Li_2O_2 and TEGDME with different concentrations of DBHQ, the X-ray diffraction (XRD) patterns point out that the crystallinity of the Li_2O_2 increases with the concentration of DBHQ due to the recrystallization of the dissolved Li_2O_2 through Ostwald ripening (Figure 2g), demonstrating Li_2O_2 can be well dissolved by the DBHQ. For investigating the solvating

ability of DBHQ toward Li^+, ^7Li NMR and Fourier transform infrared (FT-IR) spectroscopy measurements were performed. The addition of DBHQ makes the signals of ^7Li shift upfield (Figure 2h), which can be ascribed to the reinforced magnetic shielding effect around the electron-deficient Li^+ due to the increase of electron density from the electron-donating O atom of the hydroxyl groups (−OH) in DBHQ (Figure 1f). FT-IR spectra also evidence that the DBHQ induced changes of the Li^+ solvation structure. With the addition of DBHQ into the electrolytes of 1 M $LiCF_3SO_3$-TEGDME, the peaks of C−H bending vibration shift closer to the pure TEGDME solvent, revealing DBHQ can compete with TEGDME to solvate Li^+ with the liberation of free TEGDME solvent from the solvation structure of $[Li(TEGDME)_x]^+$ (Figure 2i). The phenomenon of DBHQ-induced competitive coordination with Li^+ have also been observed in other absorption spectra (Figure S4, Supporting Information) and the possibly optimized structures of DBHQ:Li^+ and DBHQ:TEGDME (Figure S5, Supporting Information). Given that the extremely unstable feature of the
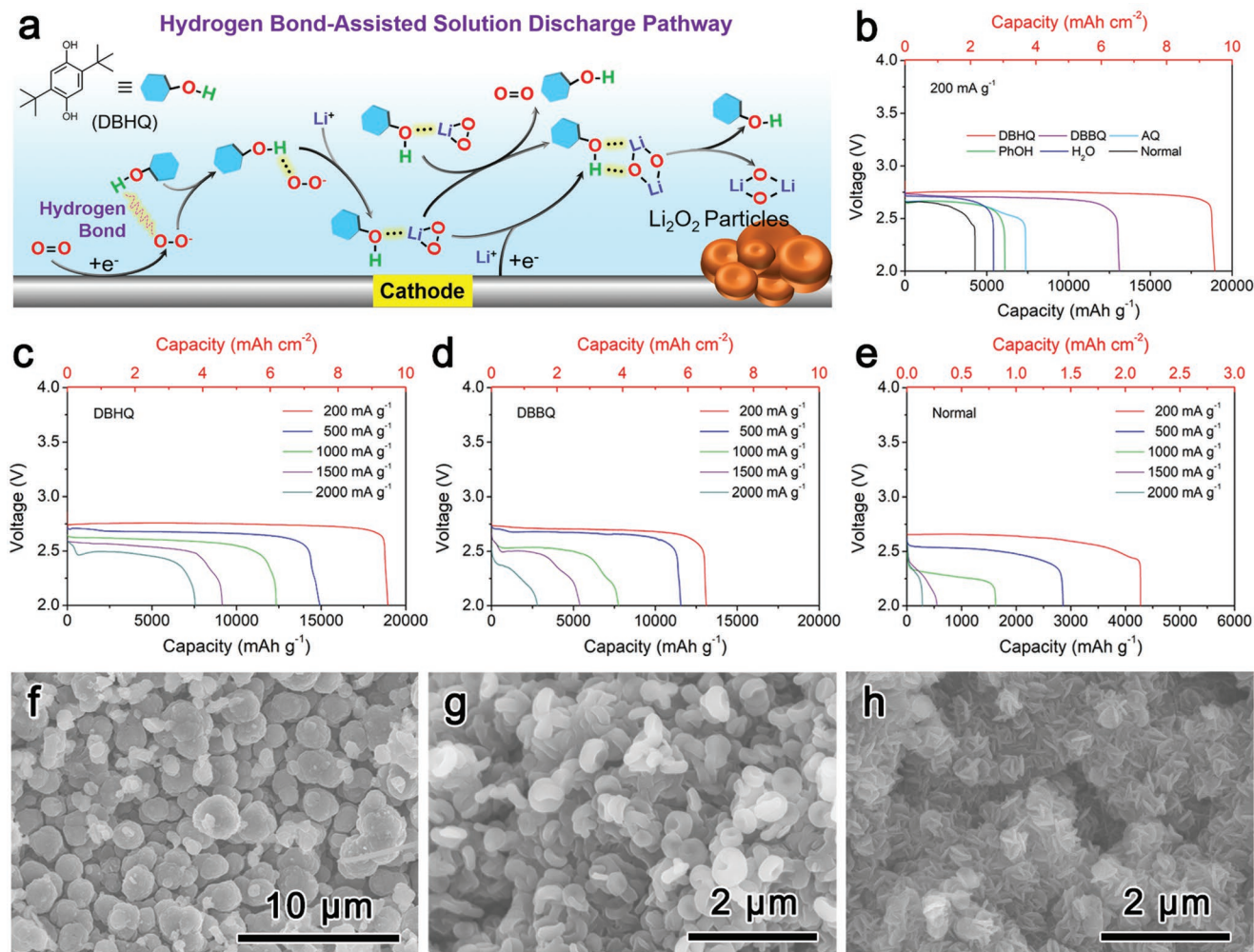

Figure 3. a) Schematic illustration of the hydrogen-bond-assisted solution discharge pathway with DBHQ. b) Galvanostatic discharge profiles of the Li–O_2 batteries with different additives at 200 mA g^{-1}. c–e) Rate performance of the Li–O_2 batteries with 50×10^{-3} M DBHQ (c), 50×10^{-3} M DBBQ (d), and without additive (e). f–h) SEM images of the discharged cathodes with 50×10^{-3} M DBHQ (f), 50×10^{-3} M DBBQ (g), and without additive at 200 mA g^{-1} (h).

LiO_2[17] and the lowest solvating Gibbs free energy of DBHQ toward LiO_2, it is a challenging task to characterize the solvating propensity of DBHQ toward LiO_2. The above experimental evidences are in good accordance with the DFT calculation results and demonstrate that DBHQ can well solvate O_2^-, Li_2O_2 and Li^+, particularly for O_2^- and Li_2O_2 through hydrogen bonding interaction (O—H···O), thus facilitating the solution-mediated discharge process. The schematic illustration of the hydrogen-bond-assisted solution discharge pathway in Li–O_2 battery is shown in **Figure 3**a.

Subsequently, galvanostatic discharge tests were carried out to check the enhanced discharge performance of the Li–O_2 batteries in the presence of DBHQ. And the reported additives with improved discharge performance were also brought in these tests for comparison, such as 2,5-di-tert-butyl-1,4-benzoquinone (DBBQ),[6] anthraquinone (AQ),[10b] phenol (PhOH),[11b] and H_2O.[2e] All the concentrations of the additives used in subsequent tests were controlled at 50×10^{-3} м. As indicated in Figure 3b and Figures S8–S10, Supporting Information, the discharge capacity of the Li–O_2 battery with DBHQ is more than fourfold larger than that of the battery with normal electrolyte (18 945 mAh g^{-1} vs 4278 mAh g^{-1}), which is even much higher than that of the battery with the state-of-the-art reduction mediator of DBBQ (13 111 mAh g^{-1}). It should be noted that the areal capacity (i.e., 9.47 mAh cm^{-2}) delivered here by DBHQ is the highest value when compared to the reported Li–O_2 batteries with an additive (Table S10, Supporting Information). Then in-depth analysis on Li–O_2 batteries with DBHQ, DBBQ, or without additive was further conducted. The Li–O_2 battery with DBHQ shows the best rate capability during discharge, and it can even maintain a capacity

of 7557 mAh g^{-1} at 2000 mA g^{-1} (Figure 3c), while the batteries with DBBQ and without additive only deliver the capacities of 2796 and 282 mAh g^{-1} (Figure 3d,e), respectively. The solution discharge promoted by DBHQ and DBBQ can be clearly evidenced by scanning electron microscopy (SEM). For the batteries with DBBQ and without additive, only small toroidal (≈500 nm) and flake-type discharge products deposit on the cathodes (Figure 3g,h), respectively. Whereas with the presence of DBHQ, micrometer-sized toroidals (2–3 µm) are observed (Figure 3f). The outstanding ORR performance for discharge capacity and rate capability endowed by DBHQ can be attributed to the hydrogen-bond-assisted solution discharge pathway in Li–O_2 batteries. The unique efficacy of this approach can be also successfully extended to other additives with −OH or −NH groups, like alkanol, butylated hydroxytoluene (BHT), NH_4^+, alkylamine, and aniline, which the discharge capacities are greatly enhanced with the incorporation of these additives (**Figure 4**a), convincingly manifesting the universality of the hydrogen-bond-assisted solution discharge approach.

The discharge products on the cathode with DBHQ are identified to be Li_2O_2 from the XRD patterns (Figure 4b) and FT-IR spectra (Figure 4c), signifying that Li_2O_2 is stable against DBHQ, which is well coincident with the previous solubility tests (Figure 2g) and thermodynamic analysis of DFT calculations (Table S11, Supporting Information). Different from the relative pure phase of Li_2O_2 with DBHQ, there are also some small characteristic peaks of the lithium carboxylates/carbonate on the discharged cathode with DBBQ, especially on the one without additive (Figure 4c). The DBHQ rendered less parasitic products can be further supported by the ^1H NMR spectra, in which the battery with DBHQ shows the lowest content of
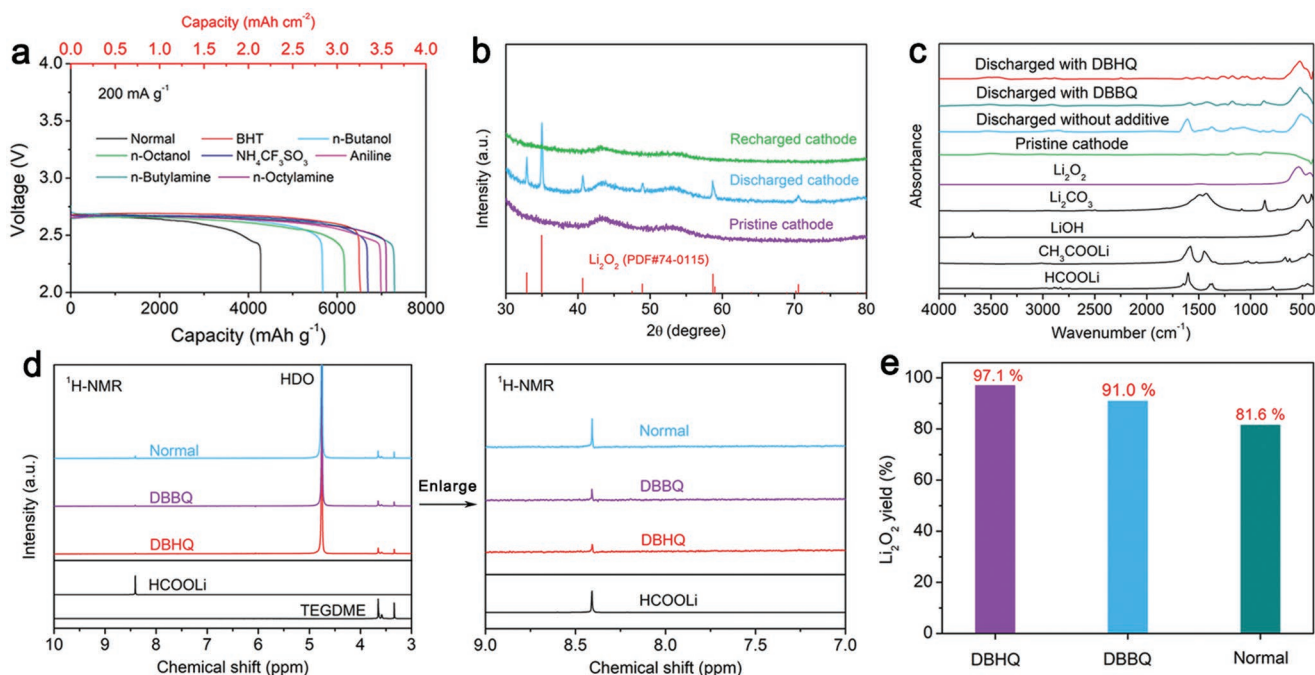
**Figure 4.** a) Galvanostatic discharge profiles of the Li–O_2 batteries with 50×10^{-3} м different additives at 200 mA g^{-1}. b) XRD patterns of the pristine, discharged, and recharged cathodes with 50×10^{-3} м DBHQ. c) FT-IR and d) ^1H NMR spectra of the discharged cathodes with different electrolytes. e) The Li_2O_2 yields in different electrolytes determined by photometric analysis.

HCOOLi (Figure 4d). To further confirm this, the Li_2O_2 yields of the Li–O_2 batteries after discharge with different electrolytes were quantitatively analyzed by $TiOSO_4$-based UV/vis spectroscopic titrations (Figures S11 and S12, Supporting Information). The battery with DBHQ delivers an ultrahigh Li_2O_2 yield of 97.1% (Figure 4e), which is the highest value for the Li–O_2 batteries with additives up to date (Table S12, Supporting Information), while the batteries with DBBQ and without additive show relatively lower Li_2O_2 yields of 91.0% and 81.6% (Figure 4e), respectively. The elevated stability of the battery with DBHQ can be owed to the depressed reactivity of the reduced oxygen-containing species (O_2^-, LiO_2, and Li_2O_2) through solvation by the antioxidative DBHQ, consequently decreasing the free-radicals-induced cathode and electrolyte decomposition with less byproducts.

Thanks to the high stability toward the reduced oxygen-containing species and the intensified solution discharge endowed by the DBHQ, the Li–O_2 battery with DBHQ will certainly show better cycling performance. RuO_2 nanoparticles decorated CNTs were employed as high-efficiency catalysts to lower down the charge overpotential here (Figures S13–S18, Supporting Information).[2d,18] As shown in **Figure 5**a, the Li–O_2 battery with 50×10^{-3} M DBHQ can operate 161 cycles with a fixed capacity of 1000 mAh g^{-1} at 500 mA g^{-1}, but those batteries with 50×10^{-3} M DBBQ and without additive can only sustain 141 and 115 cycles (Figure 5c,e), respectively. Furthermore, it can give full play to the advantages of the DBHQ when cycling Li–O_2 batteries to high limited capacity at high rate. Increasing the cycling capacity to 3000 mAh g^{-1} at 1000 mA g^{-1}, the Li–O_2 battery with DBHQ can still operate 57 cycles (Figure 5b), while those batteries with DBBQ and without additive can only run for 31 and 9 cycles (Figure 5d,f), respectively, manifesting that the DBHQ-induced high stability and solution discharge can not only improve the ORR kinetics for elevating discharge
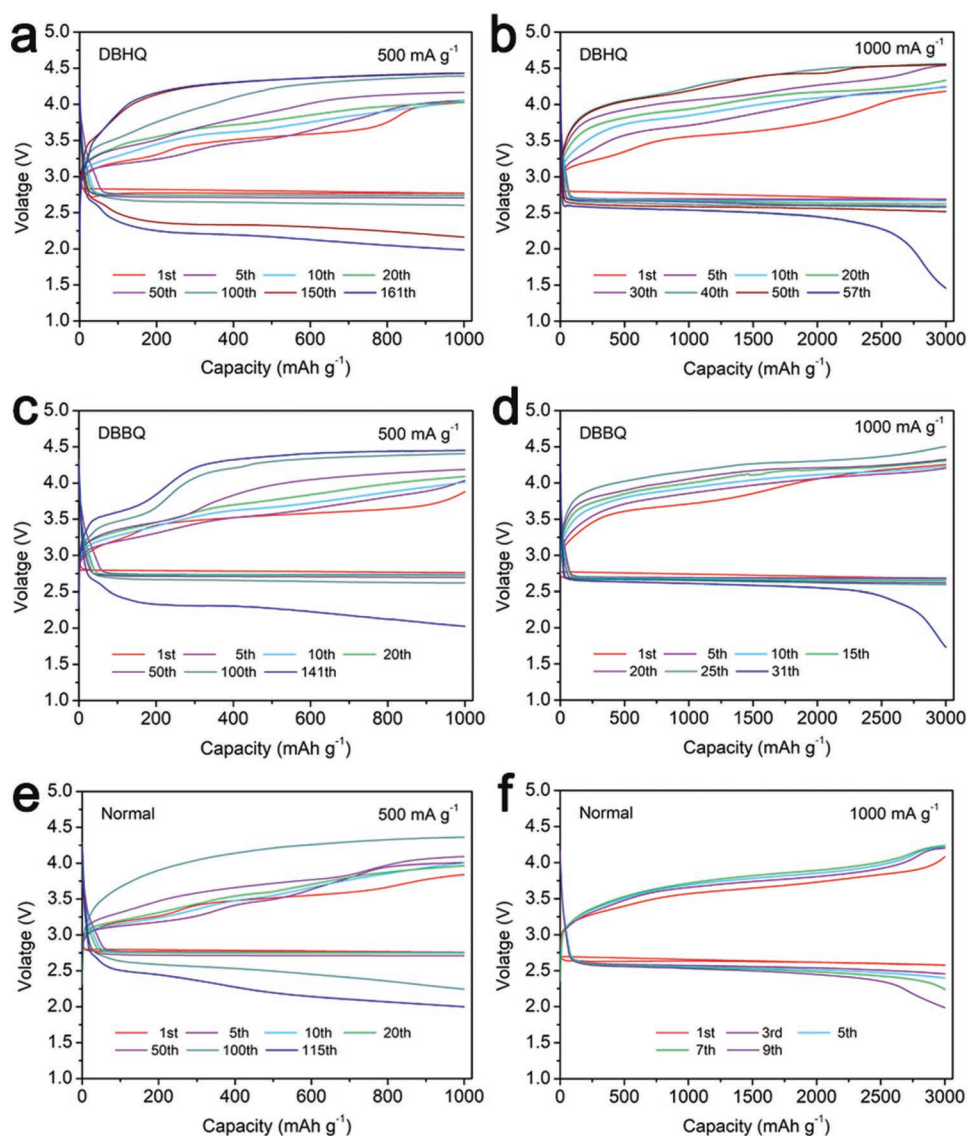
Figure 5. a–f) Cycling voltage profiles of the Li–O_2 batteries with 50×10^{-3} M DBHQ (a,b), 50×10^{-3} M DBBQ (c,d), and without additive (e,f) at 1000 mAh g^{-1} and 500 mA g^{-1} (a,c,e) or 3000 mAh g^{-1} and 1000 mA g^{-1} (b,d,f).
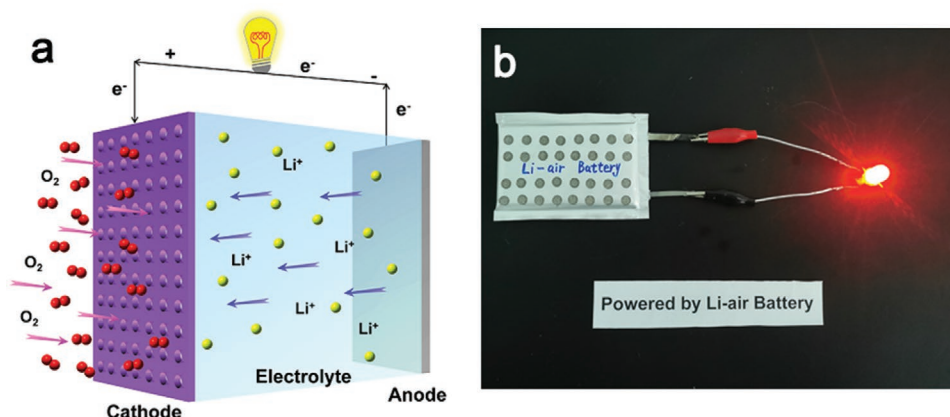
Figure 6. a) Schematic representation of the Li–O$_2$ battery during discharge. b) Operation test of the LED bulb powered by a pouch-type Li–air cell.

capacity and rate capability, but also boost the cycling lifetime of Li–O$_2$ battery. Additionally, based on the typical configuration of the aprotic Li–O$_2$ battery shown in **Figure 6**a, a pouch Li–air cell was fabricated. It is clear that the Li–air cell could work well to glow the red light-emitting diode (LED) bulb (Figure 6b), exhibiting some practical application prospects.

3. Conclusions

We have introduced DBHQ, a kind of stable antioxidant with inert hydroxyl groups, as a new liquid catalyst for Li–O$_2$ batteries to promote the solution-mediate discharge process. On the one hand, the hydroxyl groups in DBHQ can efficiently initiate the solution discharge through hydrogen-bond-assisted solvation of the O$_2^-$ and Li$_2$O$_2$ (O—H···O), thereby significantly increasing the discharge capacity to more than fourfold larger than the battery with normal electrolyte. The areal capacity enabled by DBHQ here is also the highest one ever reported for the Li–O$_2$ batteries with an electrolyte additive. On the other hand, the reduced oxygen-containing species (O$_2^-$, LiO$_2$, and Li$_2$O$_2$) can be stabilized by the DBHQ for its solvating and antioxidative features, thus resulting in a significant improvement of the nucleophilic stability for cathode and electrolyte and consequently achieving the highest Li$_2$O$_2$ yield (97.1%) among all the Li–O$_2$ batteries with additives. As a result, the Li–O$_2$ battery with DBHQ exhibits a satisfactory rate capability and cycling performance. Importantly, our concept of hydrogen-bond-assisted solution discharge can be successfully extended to other additives with —OH or —NH groups, indicating its universality.

Supporting Information

Supporting Information is available from the Wiley Online Library or from the author.

Conflict of Interest

The authors declare no conflict of interest.

Data Availability Statement

The data that support the findings of this study are available from the corresponding author upon reasonable request.

[1] K. M. Abraham, Z. Jiang, *J. Electrochem. Soc.* **1996**, *143*, 1.

[2] a) Z. Peng, S. A. Freunberger, Y. Chen, P. G. Bruce, *Science* **2012**, *337*, 563; b) X. Chi, M. Li, J. Di, P. Bai, L. Song, X. Wang, F. Li, S. Liang, J. Xu, J. Yu, *Nature* **2021**, *592*, 551; c) M. Asadi, B. Sayahpour, P. Abbasi, A. T. Ngo, K. Karis, J. R. Jokisaari, C. Liu, B. Narayanan, M. Gerard, P. Yasaei, X. Hu, A. Mukherjee, K. C. Lau, R. S. Assary, F. Khalili-Araghi, R. F. Klie, L. A. Curtiss, A. Salehi-Khojin, *Nature* **2018**, *555*, 502; d) J. L. Ma, F. L. Meng, Y. Yu, D. P. Liu, J. M. Yan, Y. Zhang, X. B. Zhang, Q. Jiang, *Nat. Chem.* **2019**, *11*, 64; e) N. B. Aetukuri, B. D. McCloskey, J. M. Garcia, L. E. Krupp, V. Viswanathan, A. C. Luntz, *Nat. Chem.* **2015**, *7*, 50; f) X. He, X. Liu, Q. Han, P. Zhang, X. Song, Y. Zhao, *Angew. Chem., Int. Ed.* **2020**, *59*, 6397; g) Z. Zhu, X. Shi, G. Fan, F. Li, J. Chen, *Angew. Chem., Int. Ed.* **2019**, *58*, 19021.

[3] L. Johnson, C. Li, Z. Liu, Y. Chen, S. A. Freunberger, P. C. Ashok, B. B. Praveen, K. Dholakia, J. M. Tarascon, P. G. Bruce, *Nat. Chem.* **2014**, *6*, 1091.

[4] Z. Peng, S. A. Freunberger, L. J. Hardwick, Y. Chen, V. Giordani, F. Barde, P. Novak, D. Graham, J. M. Tarascon, P. G. Bruce, *Angew. Chem., Int. Ed.* **2011**, *50*, 6351.

[5] D. Zhai, H. H. Wang, K. C. Lau, J. Gao, P. C. Redfern, F. Kang, B. Li, E. Indacochea, U. Das, H. H. Sun, H. J. Sun, K. Amine, L. A. Curtiss, *J. Phys. Chem. Lett.* **2014**, *5*, 2705.

[6] X. Gao, Y. Chen, L. Johnson, P. G. Bruce, *Nat. Mater.* **2016**, *15*, 882.

[7] Y. Zhang, L. Wang, X. Zhang, L. Guo, Y. Wang, Z. Peng, *Adv. Mater.* **2018**, *30*, 1705571.

[8] M. J. Lacey, J. T. Frith, J. R. Owen, *Electrochem. Commun.* **2013**, *26*, 74.

[9] a) C. M. Burke, V. Pande, A. Khetan, V. Viswanathan, B. D. McCloskey, *Proc. Natl. Acad. Sci. USA* **2015**, *112*, 9293; b) D. G. Kwabi, V. S. Bryantsev, T. P. Batcho, D. M. Itkis, C. V. Thompson, Y. Shao-Horn, *Angew. Chem., Int. Ed.* **2016**, *55*, 3129.

[10] a) Q. Xiong, G. Huang, X. B. Zhang, *Angew. Chem., Int. Ed.* **2020**, *59*, 19311; b) P. Zhang, L. Liu, X. He, X. Liu, H. Wang, J. He, Y. Zhao, *J. Am. Chem. Soc.* **2019**, *141*, 6263; c) S. Wu, N. Qin, H. Zhang, C. Wei, Z. Wang, W. Luo, Y. Li, H. Wang, K. Zhang, Q. Wang, Z. Lu, *Chem. Commun.* **2022**, *58*, 1025; d) M. Xu, J. Yang, C. Sun, Y. Cui, L. Liu, H. Zhao, B. Liang, *J. Mater. Sci.* **2020**, *56*, 1328; e) S. Yan, J. Yu, B. Zhu, K. Qiao, X. Cai, X. Yuan, C. Li, *ECS J. Solid State Sci. Technol.* **2021**, *10*, 011002.

[11] a) Y. Qiao, S. Wu, J. Yi, Y. Sun, S. Guo, S. Yang, P. He, H. Zhou, *Angew. Chem., Int. Ed.* **2017**, *56*, 4960; b) X. Gao, Z. P. Jovanov, Y. Chen, L. R. Johnson, P. G. Bruce, *Angew. Chem., Int. Ed.* **2017**, *56*, 6539; c) Y. G. Zhu, Q. Liu, Y. Rong, H. Chen, J. Yang, C. Jia, L. J. Yu, A. Karton, Y. Ren, X. Xu, S. Adams, Q. Wang, *Nat. Commun.* **2017**, *8*, 14308.

[12] E. Arunan, G. R. Desiraju, R. A. Klein, J. Sadlej, S. Scheiner, I. Alkorta, D. C. Clary, R. H. Crabtree, J. J. Dannenberg, P. Hobza, H. G. Kjaergaard, A. C. Legon, B. Mennucci, D. J. Nesbitt, *Pure Appl. Chem.* **2011**, *83*, 1637.

[13] U. Sayin, Ö. Dereli, E. Türkkan, H. Yüksel, M. Birey, *Radiat. Phys. Chem.* **2011**, *80*, 38.

[14] M. J. Frisch, G. W. Trucks, H. B. Schlegel, G. E. Scuseria, M. A. Robb, J. R. Cheeseman, G. Scalmani, V. Barone, G. A. Petersson, H. Nakatsuji, X. Li, M. Caricato, A. V. Marenich, J. Bloino, B. G. Janesko, R. Gomperts, B. Mennucci, H. P. Hratchian, J. V. Ortiz, A. F. Izmaylov, J. L. Sonnenberg, D. Williams-Young, F. Ding, F. Lipparini, F. Egidi, J. Goings, B. Peng, A. Petrone, T. Henderson, D. Ranasinghe, et al., Gaussian 16A, Gaussian, Inc., Wallingford CT, USA **2016**.

[15] T. Lu, F. Chen, *J. Comput. Chem.* **2012**, *33*, 580.

[16] a) J. Herranz, A. Garsuch, H. A. Gasteiger, *J. Phys. Chem. C* **2012**, *116*, 19084; b) D. G. Kwabi, M. Tulodziecki, N. Pour, D. M. Itkis, C. V. Thompson, Y. Shao-Horn, *J. Phys. Chem. Lett.* **2016**, *7*, 1204.

[17] X. Zhang, L. Guo, L. Gan, Y. Zhang, J. Wang, L. R. Johnson, P. G. Bruce, Z. Peng, *J. Phys. Chem. Lett.* **2017**, *8*, 2334.

[18] J. J. Xu, Z. W. Chang, Y. Wang, D. P. Liu, Y. Zhang, X. B. Zhang, *Adv. Mater.* **2016**, *28*, 9620.